AIP | Journal of Applied Physics

Theoretical and experimental approach on dielectric properties of ZnO nanoparticles and polyurethane/ZnO nanocomposites

T. S. Velayutham, W. H. Abd Majid, W. C. Gan, A. Khorsand Zak, and S. N. Gan

Citation: J. Appl. Phys. **112**, 054106 (2012); doi: 10.1063/1.4749414
View online: http://dx.doi.org/10.1063/1.4749414
View Table of Contents: http://jap.aip.org/resource/1/JAPIAU/v112/i5
Published by the American Institute of Physics.

Theoretical and experimental approach on dielectric properties of ZnO nanoparticles and polyurethane/ZnO nanocomposites

T. S. Velayutham,[1,a)] W. H. Abd Majid,[1] W. C. Gan,[1] A. Khorsand Zak,[1] and S. N. Gan[2]
[1]*Low Dimensional Materials Research Centre, Physics Department, University of Malaya, 50603 Kuala Lumpur, Malaysia*
[2]*Chemistry Department, University of Malaya, 50603 Kuala Lumpur, Malaysia*

(Received 2 March 2012; accepted 9 August 2012; published online 10 September 2012)

ZnO nanoparticles (ZnO-NPs) were synthesized by a new, simple sol-gel method in gelatin media (particle size of ZnO ≈ 30 to 60 nm). Polyurethane/ZnO nanocomposites thin films (PU/ZnO-NPs) were prepared by mixing the ZnO-NPs into PU prepolymer. The nanocomposites were structurally characterized using Fourier transmission infrared (FTIR) spectroscopy. The interaction between ZnO-NPs and PU matrix is studied by analyzing the differences in C=O region and N-H region of FTIR spectra. The morphology of ZnO and PU/ZnO nanocomposites were assessed using transmission electron micrograph, TEM, and field emission scanning electron microscope, FESEM, respectively. The dielectric properties of ZnO-NPs were attributed to the interfacial and orientation polarization. Measurement is reported for the real and imaginary parts of the ac conductivity of ZnO-NPs in the frequency range of 10 to 10^6 Hz in the temperature range 298–478 K. The experimental results are interpreted in terms of the classical correlated-barrier hopping theory. In addition, the dielectric properties of PU/ZnO nanocomposites (0–15 vol. % filler concentration) were analyzed with respect to frequency. Quantitative analysis based on mixing laws for two-phase spherical dispersion system such as Lichtenecker, Maxwell, Jayasundere and Smith, and Yamada equations was used to predict the effective permittivity accurately up to 15 vol. % of ZnO in PU matrix. © *2012 American Institute of Physics*. [http://dx.doi.org/10.1063/1.4749414]

I. INTRODUCTION

Zinc oxide (ZnO) is a promising material for many applications such as nano-scale electronic and optoelectronic device because of its wide band gap ($E_g = 3.3$ eV) in the near UV spectral region and large exciton binding energy (60 meV).[1] ZnO can be made in various types of one dimensional nanostructure such as nanoparticle, nanorods, nanotubes, and nanowires; thus it is attractive for gas and chemical sensing,[2] micro lasers, and memory arrays applications.[3] Furthermore, it can be used in many other applications such as large area flat panel displays, solar cells,[4] transparent conductive coatings,[5] varistors, piezoelectric and transparent electrodes, bio sensors, etc. ZnO nanostructures have also been studied as conductive fillers in polymers with high electrical permittivity and these nanostructures have received increasing attention for their potential application in high charge-storage capacitors.[1]

Polyurethane (PU) is a versatile polymer[6] due to its micro phase-separated structure attributed from thermodynamic incompatibility between hard and soft segments.[7,8] By combining the advantages of both properties of PU (e.g., versatility, flexibility, ductility, dielectric property) and ZnO (e.g., rigidity, high thermal stability, strength, hardness, high refractive index) as well as large interfacial coupling between the nano-sized particles, PU/ZnO nanocomposites have potential industrial applications such as sensors, actuators, and integrated electronic devices.

It is a common practice to functionalize the ZnO nanoparticles (ZnO-NPs) with surfactant or a coupling agent to stabilize and render the NPs compatible with the polymer matrix. However, in this case, the ZnO-NPs without surface modification are used. They are compatible with PU because there is a special interaction between PU and ZnO-NPs. The most likely reason for the special interaction is the reaction between the surface hydroxyl groups of the ZnO-NPs and the isocyanate groups of the polyurethane pre-polymer.[9] The isocyanates groups react with ZnO-NPs creating strong hydrogen bonding in the PU matrix which could improve the compatibility between ZnO-NPs and PU, thus yielding better dispersion.

Several literatures investigating the structural and mechanical properties of PU/ZnO nanocomposite have been reported.[7,9–12] In 2005, Zheng *et al*. have studied the disruption of self-assembly and altered mechanical behavior in PU/ZnO nanocomposites,[9] and in 2006, the same group has reported the mechanical phase separation and mechanical responses of polyurethane nanocomposites.[7] Mishra *et al*.[10] have studied the structural characterization, degree of branching calculation, and structure to property correlation study of hyperbranched polyester based PU/ZnO hybrid coatings, whereas Mishra *et al*.[11] explored the phase mixing behavior of nano ZnO in PU matrix. Electrical and dielectric properties of PU/ZnO nanocomposites have not yet been studied in detail.

The present paper addresses the issues on the dielectric properties of the ZnO-NPs and PU/ZnO nanocomposites by means of experimental and theoretical approach. Compatibility of PU matrix and ZnO by analyzing the differences in C=O

[a)]Electronic addresses: t_selvi@um.edu.my and thamil_selvi@yahoo.com. Tel.: +60379674147. Fax: +60379674146.

region and N-H region of FTIR spectra is discussed and supported by the morphology of the materials. An illustration of the PU/ZnO nanocomposite is proposed to elucidate the micro phase separation in PU. The frequency spectra of the complex permittivity over a broad frequency range for the ZnO-NPs were measured. Charge transport properties of the ZnO-NPs as a function of temperature and frequency are also investigated. PU/ZnO nanocomposites are the most promising embedded capacitor material for organic substrates application.[13–16] Besides, the dielectric constants of PU/ZnO composite with various concentrations of ZnO nanoparticles were measured. Predicting the effective permittivity of PU/ZnO nanocomposites is very important for designing the composite materials according to the end-use. Hence, the experimental data were fitted to several theoretical equations (Lichtenecker, Maxwell, Jayasundere and Smith, and Yamada) to find the equation useful for the prediction of the effective dielectric permittivity of the PU/ZnO nanocomposites.

II. EXPERIMENTAL PROCEDURE

A. Materials

Oleic acid (purity 99.5%) and glycerol (purity 99.5%) were obtained from Cognis Oleochemical (M) Sdn Bhd. (Malaysia). Phthalic anhydride, PA (P.T. Petrowida, Indonesia), and toluene diisocyanate, TDI (Aldrich, USA), were used as received. Acetone (Merck, Germany) and toluene (JT Baker, USA) were used as solvent and dried with an activated molecular sieve overnight before use. Silicone surfactant (Air Products, USA) and defoamer (BYK Chemie, Germany) were used in the preparation of PU prepolymer. The ZnO nanoparticles were synthesized by a new, simple sol-gel method in gelatin media and the particles sizes were ranging from 30 to 60 nm.[17] The ZnO nano powders were dried at 130° for 24 h to remove the absorbed water prior to any characterization or use.

B. Preparation

ZnO-NPs were prepared by dissolving zinc nitrate in distilled water and stirred for 30 min. Meanwhile gelatin was dissolved in distilled water and stirred to achieve a clear gelatin solution. Zinc nitrate solution was added to the gelatin solution and the solution was moved to water bath at temperature 80 °C. After stirring for 12 h to obtain a brown resin, the temperature of the resin was reduced to room temperature and the resin became hard. The final product was calcined as reported in Ref. 17. ZnO pellets for dielectric measurements (diameter 13 mm and thickness 2–5 mm) were prepared with a very small amount of polyethylene glycol (Mw = 600) as binder in the NPs and compressed by applying a pressure of 500 bar in a hydraulic press.

PU nanocomposite was prepared by *in situ* suspension polymerization. Polyol was prepared by using oleic acid (400 g), glycerol (256 g), and PA (338 g).[18,19] The polyol was allowed to react with TDI in the presence of solvent (toluene), surfactant, and defoamer at 80 °C over 3 h with continuous stirring. The NCO/OH ratio was maintained at 1.4. ZnO-NPs with different weight percentage (0% to 15%) were dispersed in acetone in an ultrasonic bath at room temperature for 22 min to ensure homogeneous dispersion. The dispersed ZnO-NPs were added into PU pre-polymers and mixed ultrasonically for 30 min at 60 °C.

Glass substrates were first coated with aluminium electrodes using thermal evaporator. The prepared PU/ZnO nanocomposites solutions were spin coated to produce thin films with thickness ranging from 300 nm to 500 nm. The films were left in the oven overnight at 60 °C to cure and to fully remove the solvent. The top layer of the nanocomposite films was coated with aluminium electrodes to yield metal-insulator-metal (MIM) structure with a 2 mm × 2 mm active electrode area. Silver paste was used as an electrical contact.

C. Characterization

Fourier transmission infrared (FTIR) spectra of PU/ZnO thin films were coated on dry potassium bromide (KBr) pellet recorded on (Pelkin Elmer 2000, FTIR) spectrometer with resolution setting of 4 cm^{-1} and range of 400–4000 cm^{-1}. Each sample was scanned 16 times. The ZnO-NPs were characterized by transmission electron microscope (TEM) and the surface of nanocomposites PU/ZnO-15% was examined with a field emission scanning electron microscope (FEI Quanta 200 F FESEM). AC dielectric measurement of the nanocomposites was performed with the impedance analyzer (HP 4294) in the frequency range of 10 Hz to 10^6 Hz at room temperature.

III. RESULTS AND DISCUSSION

A. FTIR analysis of PU and PU/ZnO-NPs

The IR spectra of PU and PU/ZnO nanocomposites coated on KBr disc in the zone 400–4000 cm^{-1} are shown in Fig. 1(a) and the characteristic peaks are given in Table I. The presence of ZnO is indicated by the peak at 1540 cm^{-1} which is overlapped by amide II zone.[10]

The absorption peaks in the C=O region and N-H region were expanded to distinguish differences in the urethane and urea bonding of the pure PU and PU/ZnO nanocomposites (refer to Fig. 1(b)). The absorption peaks of both regions were increasing for all ZnO concentration. However, the increment of the absorption peaks for the samples with more than 5% was small if compared with that of below 5%. In general, the special interaction between PU and ZnO-NPs is because of the reaction between the surface hydroxyl groups of the ZnO-NPs and the isocyanate groups (NCO) of the polyurethane pre-polymer. The excess isocyanate in the system is related to NCO/OH ratio of pre-polymer, where, in this case, the NCO/OH ratio is maintained at 1.4. Ideally, the reaction of NCO with the surface OH groups of the ZnO-NPs occurs from the excess isocyanate (that is, ~0.4 but in real cases it might be lower due to the reaction of isocyanate with atmosphere moisture, contaminant, etc). The saturation of absorption peaks in the C=O and N-H region above 5 wt. % is presumably because all the excess isocyanate was consumed by the reaction with the hydroxyl group and reached a saturation limit.

Extend of hydrogen bonding and micro phase separation in PU will be able to examine via analyzing the differences in C=O region and N-H region of FTIR spectra.[20]

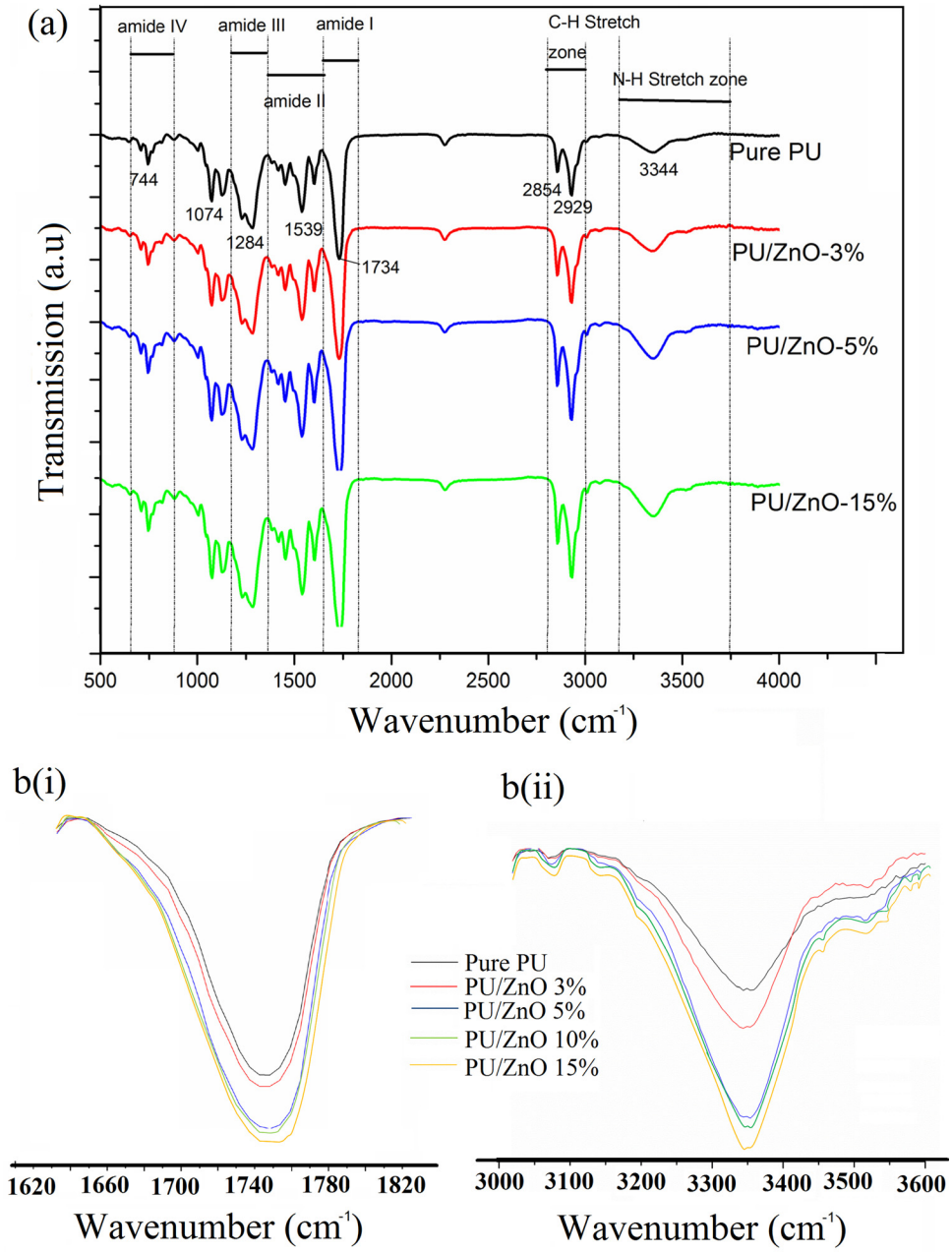

FIG. 1. (a) The FTIR spectra of PU and PU/ZnO composite thin films coated on KBr pellet and recorded at room temperature; (b) absorption peaks: (i) C=O region (ii) N-H region of various ZnO wt. % in the composites.

In order to evaluate the complex band envelopes and to identify underlying component bands in the -NH and -C=O bands region, the curve fitting simulations were performed using ORIGIN PRO 8.1 software. The N-H and C=O bands region were deconvoluted by considering peaks as Gaussian with a number of iteration to get the best fit Gaussian peak as reported in the literatures.[10,11] The maximum error associated with the fit approximate to be less than 5%.

TABLE I. FTIR characteristic band of the synthesized different PU/ZnO composites.[4,5]

Frequency (cm^{-1})	Assignment
3050–3750 cm^{-1}	NH stretching vibrations
2800–3000 cm^{-1}	CH stretching vibrations: anti-symmetric and symmetric stretching vibration mode
1600–1800 cm^{-1}	Amide I: C=O stretching vibrations
1500–1540 cm^{-1}	Amide II: C-N stretching and $\delta_{N-H} + \nu_{C-N} + \nu_{C-C}$
1200–1289 cm^{-1}	Amide III, ν_{C-N} and in-plane N-H deformation
1070–1074 cm^{-1}	C-N stretch
744 cm^{-1}	Amide IV

Figs. 2(a) and 2(b) represent the deconvoluted C=O zone and N-H zone of PU and PU/ZnO 5% films, respectively. In order to test the reproducibility of the results, for each sample with respective concentration of ZnO, three series of samples were repeated. The reproducibility of the results was ±3%. Deconvolution was performed on the IR spectra of the composites of ZnO concentrations up to 15 wt. % and the results obtained were almost similar to PU/ZnO 5%, thus the exemplifying analysis results on PU/ZnO 5% was tabulated as a representative.

The deconvolution of C=O zone displays a peak at 1676 cm^{-1} which represents free urea, two peaks at 1737 cm^{-1} and 1727 cm^{-1} which represent free urethane for PU and the peaks 1707 cm^{-1} and 1712 cm^{-1} represents hydrogen bonded

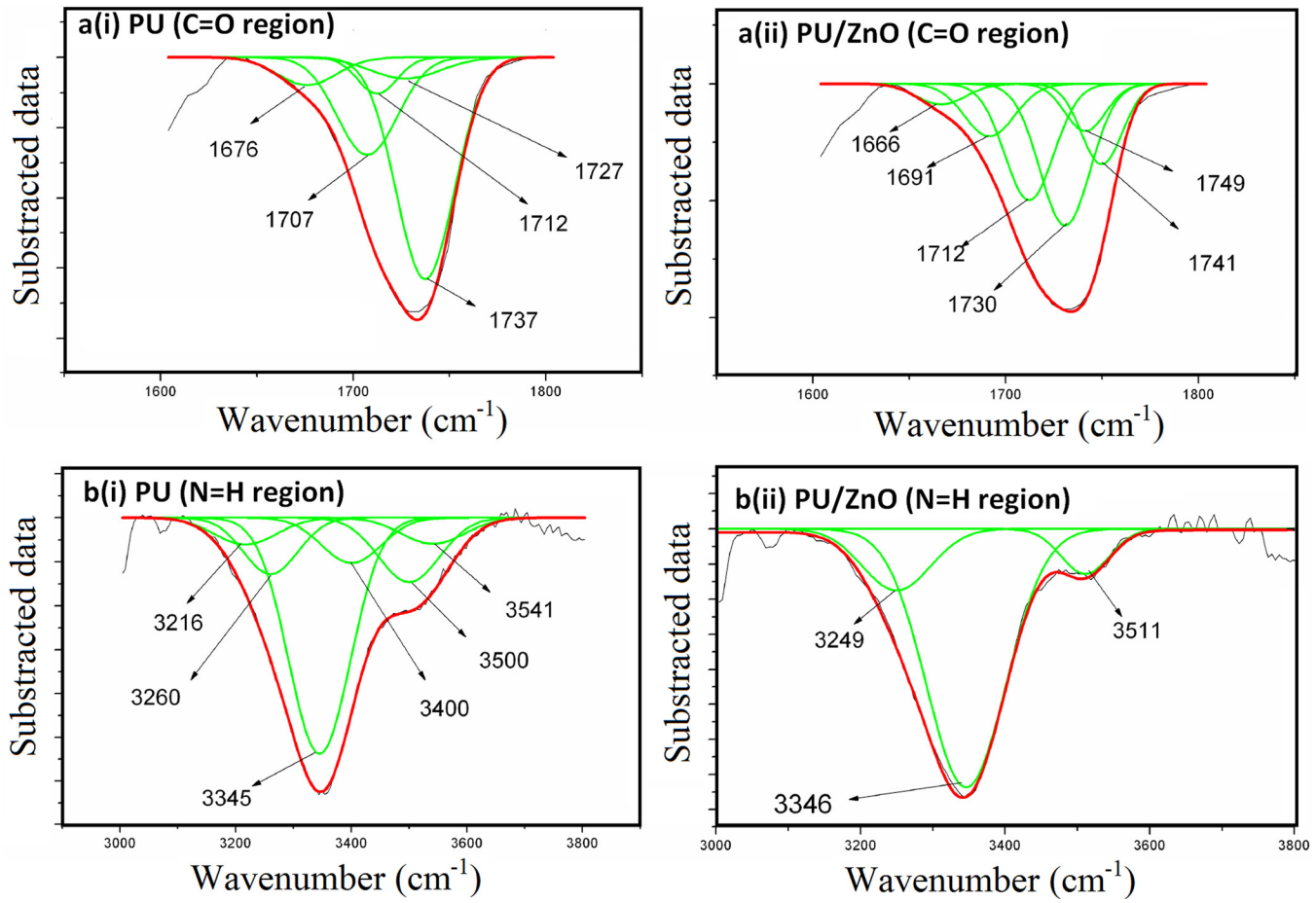

FIG. 2. FTIR peak deconvolution of (a) C=O region and (b) N-H region of PU and PU/ZnO-5% films denoted as (i) and (ii), respectively.

urethane. As for PU/ZnO 5% composites, the peaks 1666 cm^{-1}, 1691 cm^{-1}, 1712 cm^{-1}, and 1730 cm^{-1} represent bonded urethane, medium to strong H-bonded urethane, H-bonded urethane, and free urethane, respectively.[9–11,20,21] The peak area was analyzed (as shown in Table II), and it is noted that the peak area of free urethane decreases (from 55.3 to 32.9 for PU and PU/ZnO 5%, respectively) and bonded urethane increases (combination area 31.2 contributed from peaks 1707 and 1712 of PU to combination area of 43.1 contributed from peaks 1666, 1691, and 1712 of PU/ZnO 5%) with the inclusion of ZnO. The 1707 cm^{-1} and 1712 cm^{-1} peak represent the COO^{-} group.

As for the N-H region, the peak of 3345 cm^{-1} represents H-bonded –NH (with peak area of 53.1), the peak of 3400 cm^{-1} represents H-bonded amide (with the peak area of 9.7), the peak of 3500 cm^{-1} represents free amide (peak area of 14.2) and 3541 cm^{-1} (integrated peak area of 5.9) represents free N-H for pure PU.

As for PU/ZnO the peak of 3346 cm^{-1} represents H-bonded NH type II with integrated area of 73.6 (the

TABLE II. De-convoluted (a) C=O region and (b) N-H region and its integrated peak area for pure PU and PU/ZnO composites.

PU		PU/ZnO-5%	
Peak (cm^{-1})	Integrated area	Peak (cm^{-1})	Integrated area
		(a) C=O region	
1676 (free urea)	7.02	1666 (H-bonded urethane)	4.64
1707 (H-bonded urethane)	25.09	1691 (medium to strong H-bonded urethane)	12.18
1737 (free urethane)	55.34	1712 (H-bonded urethane)	26.28
1712 (H-bonded urethane)	6.12	1730 (free urethane group)	32.91
1727 (free urethane)	6.41		
		(b) N=H region	
3345 (H-bonded NH type II)	53.09	3249 (free NH stretching zone)	14.99
3400 (H-bonded amide)	9.72	3346 (H-bonded NH type II)	73.63
3500 (free amide)	14.20	3511 (free amide)	7.79
3541 (free N-H)	6.93		

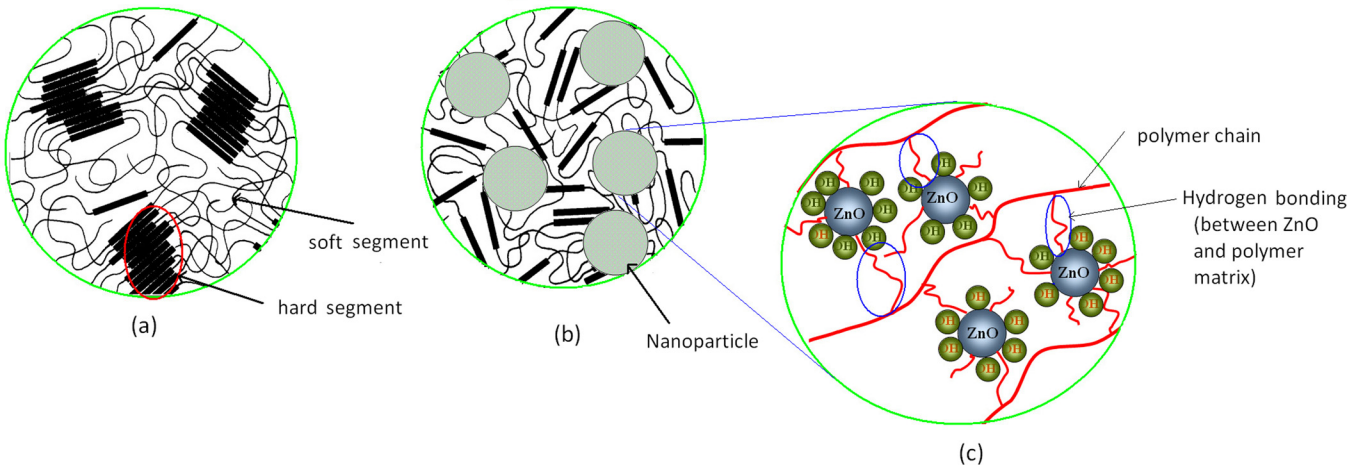

FIG. 3. Schematic representations of PU and PU/ZnO nanocomposites at room temperature: (a) phase separated morphology of pure PU due to soft and hard segments, (b) disruption of phase separation due to ZnO incorporation in PU matrix, (c) nanoparticles in PU matrix.

value increased compared to pure PU) and the peak of 3511 cm^{-1} represents free amide with integrated area of 7.8 (the value decreased). It is obvious that the NH stretching region shows increment of H-bonded peak area than free amide.

The increment in the bonded urethane and H-bonded NH with ZnO inclusion from the deconvolution results suggest that the ZnO was inserted into the PU matrix and thus accredited to the disruption of the phase separation. Incorporation of ZnO-NPs increased the inter-chain association through hydrogen bonding and the result is consistent with the reported literature.[9–11,20–22] The reaction between the PU and surface hydroxyl groups on the particles is the cause of the phase disruption in PU matrix.[21] There are fewer hard phases formed in the composites (compared to neat) PU due to interaction between PU prepolymer and the surface hydroxyl groups of ZnO-NPs where each nanoparticle acts as a cross linker and constrains the polymer chain mobility, thus limits the formation of the phases. As a result, less hard phases were formed.[9] This occurrence is illustrated in schematic representation in Fig. 3.

B. Morphology study by FESEM/TEM

Figure 4(a) shows TEM micrograph of the ZnO-NPs. The ZnO-NPs were almost hexagonal in shape and the average initial sizes were ~59 nm as evidenced by the TEM micrographs. The surface morphology of the pure PU and PU/ZnO nanocomposites as obtained by FESEM with 15 vol. % of ZnO-NPs filler is shown in Figures 4(c) and 4(d), respectively.

NPs are shown as white spheres dispersed throughout the entire area examined with smooth surface finish with minimum porosity which indicates that the ZnO-NPs are evenly distributed in the PU matrix. The homogeneity of the surface indicates that there is a good compatibility between the PU matrix and ZnO-NPs surface[11] which is in agreement to the FTIR analysis and furthermore improves the electrical properties of the nanocomposites (which is reflected in the dielectric study below).

C. Impedance measurement

1. ZnO-NPs

Figure 5 shows the double logarithmic plots of (a) real and (b) imaginary components of the complex permittivity ε^* against frequency, f, for the pure ZnO-NPs at various temperatures.

The analysis of the relaxation mechanism is complicated because of the dominant influence of conduction. In order to separate the dc conduction and the relaxation, Havriliak-Negami (HN) relaxation model was used[23] to fit the experimental result. The HN function is

$$\varepsilon^* = \varepsilon_\infty + \frac{\Delta\varepsilon}{(1+(i\omega\tau)^\alpha)^\beta} + \frac{\Delta\sigma_{dc}}{i\omega}\left(1 - \frac{1}{1+(i\omega\tau_{if})^{\gamma_{if}}}\right), \quad (1)$$

where ε_∞ represent the instantaneous dielectric constant, $\Delta\varepsilon$ is the dielectric relaxation strength, τ is the relaxation time, and α and β are parameters expressing distribution of relaxation times. The third terms correspond to the conductive relaxation due to interfacial polarization, where $\Delta\sigma_{dc}$ is the dc conductivity, τ_{if} is the relaxation time, and γ_{if} is the parameters which express the distribution of relaxation times.

There are two dielectric relaxation observed in the ZnO-NPs due to interfacial and orientation polarization. From Eq. (1), the third term was used to fit the interfacial polarization and we found it occurs only at lower frequency (<10 Hz) for all the temperature investigated as shown in Figure 6. Interfacial polarization occurs because of structural inhomogeneity created by a large surface-to-volume ratio of grains. ZnO-NPs pellet is an aggregate of small crystalline grains bonded to each other and may have a number of surface defects such as dangling bonds, vacancies, and micro-pores at the grain boundaries. It is likely that when carriers meet boundary, they stay there for a while until they pass through the boundary and generate polarization. As a result, permittivity increased as the frequency decreased[1,3] and the corresponding results of the ZnO-NPs for 298 K and 478 K are shown in Figure 6.

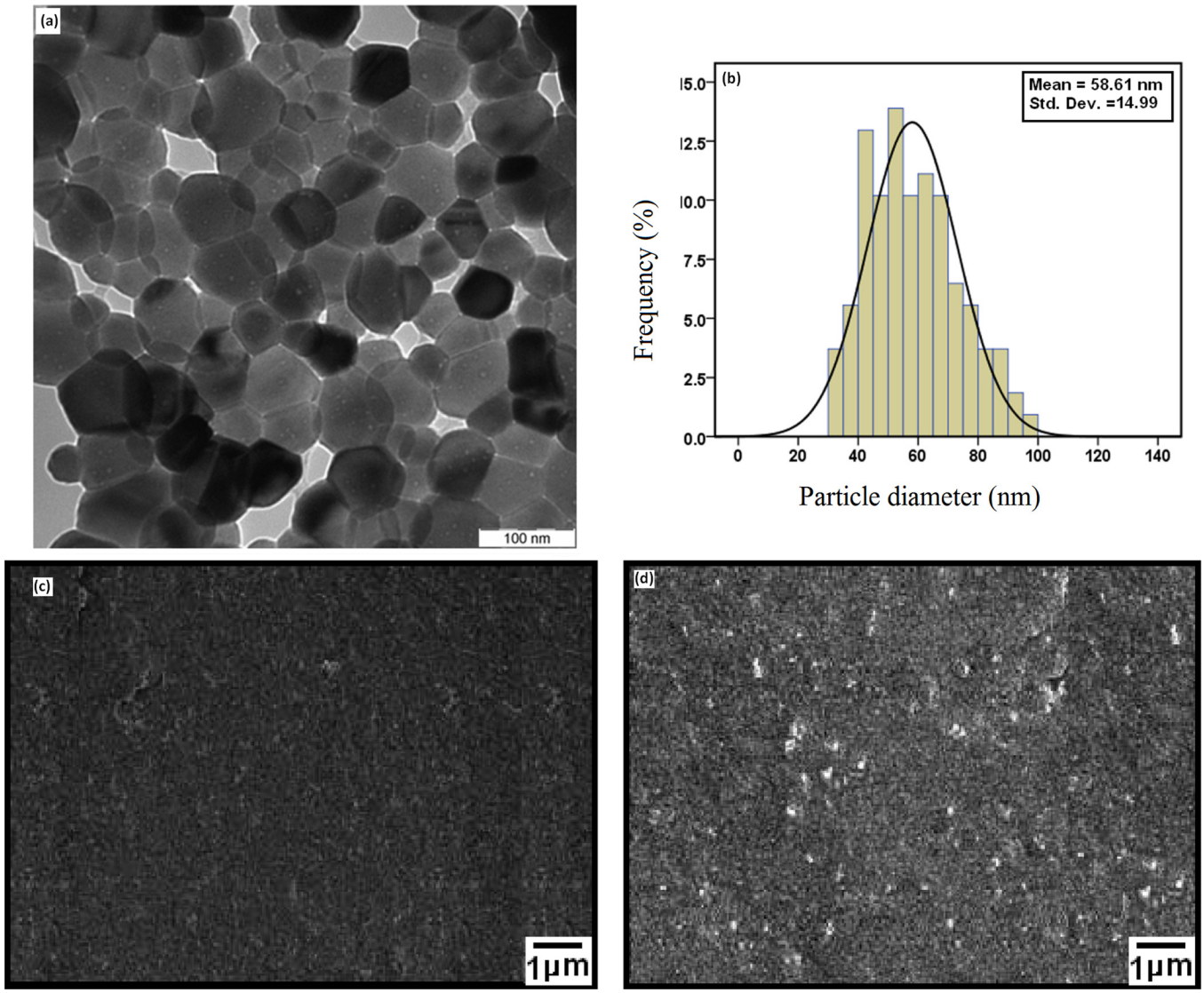

FIG. 4. TEM images of (a) ZnO nanoparticles with hexagonal shape, (b) ZnO-NPs size distribution, FESEM micrograph of (c) PU film, (d) PU/ZnO-15%.

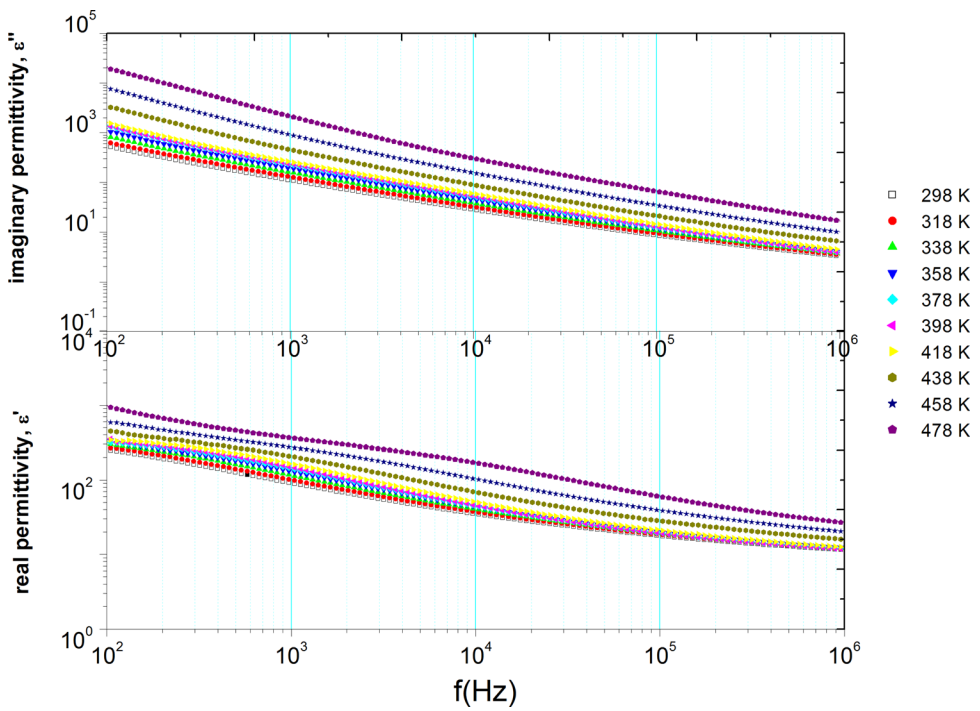

FIG. 5. (a) Real permittivity, (b) imaginary permittivity spectra of ZnO-NPs at various temperatures.

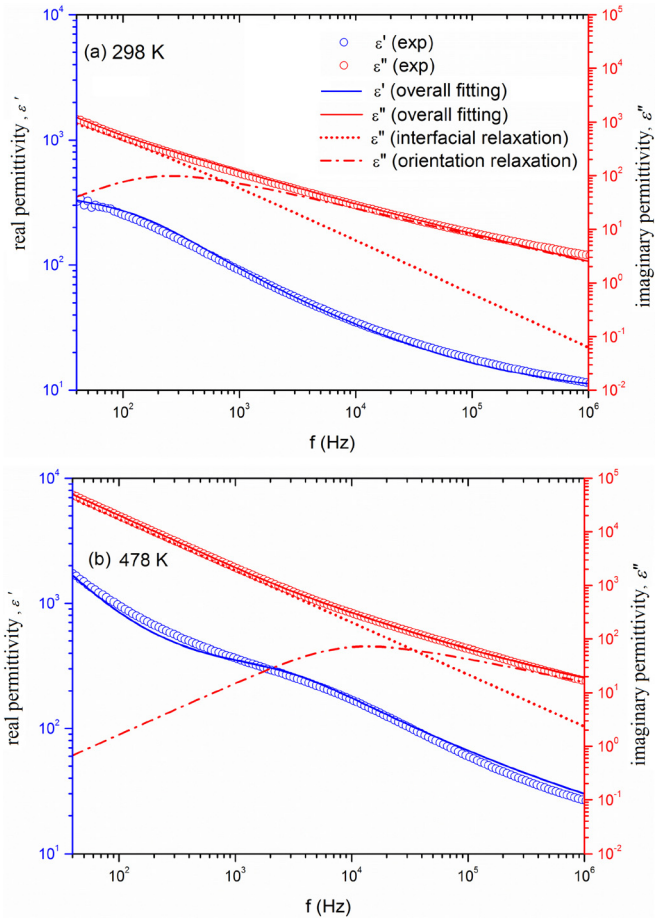

FIG. 6. Real permittivity and imaginary permittivity of ZnO at room temperature. The relaxations are due to interfacial and orientation polarizations. The best fitting curves of Eq. (1) to the data are also presented.

The orientation polarization was fitted using the first and second terms of Eq. (1). As illustrated in Figure 6, we can reproduce the observed spectra (open marks) very well using Eq. (1) (solid lines). The dashed lines show the absorption due to interfacial and orientation polarizations. The fitting parameters for the HN model at room temperature (298 K) and 478 K are $\alpha = 0.53$, $\beta = 0.95$, $\tau(s) = 0.0067$, $\Delta\varepsilon = 150$, and $\alpha = 0.45$, $\beta = 0.95$, $\tau(s) = 1.40 \times 10^{-4}$ s, and $\Delta\varepsilon = 303$.

Orientation polarization was observed at around 150 Hz at room temperature and shifted to 3.5 kHz at 478 K as shown in Figure 6. The possible source of the orientation polarization is the existence of a number of oxygen vacancies and zinc interstitials in the nanoparticles. The Zn^{2+} ions and the O^{2-} vacancies in the vicinity exchange their positions by a single jump and try to align along the direction of the field when an external field is applied.

The frequency dependence of ac conductivity of the ZnO pellet at various temperatures on a log-log scale is displayed in Figure 7(a). The red line distinguishes the dc conductivity and power law regimes. The key features of ac conductivity characteristic of the ZnO from the figure are as follows:

(i) At high frequencies ac conductivity approximates a power law relation

$$\sigma_{ac}(\omega) = A\omega^{s}, \tag{2}$$

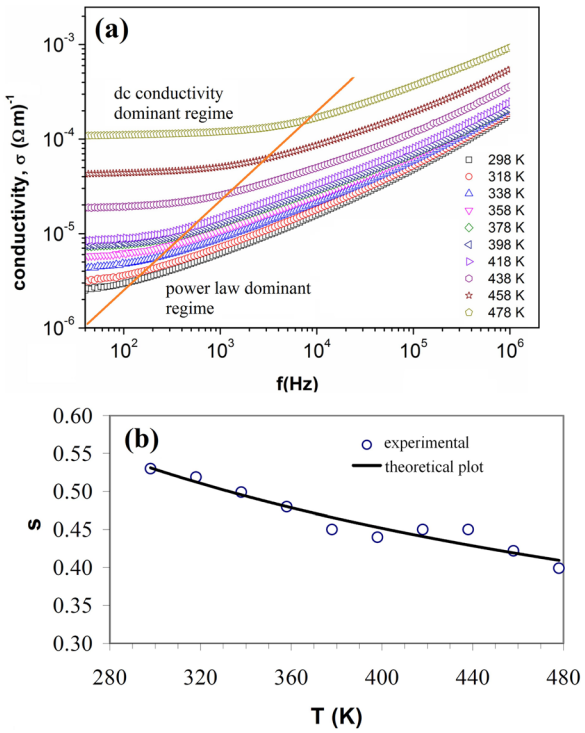

FIG. 7. (a) Conductive spectra of ZnO-NPs at various temperatures. The red line separates dc conductivity dominant region and power law dominant region based on temperature variation. (b) Temperature dependence of exponent *s*.

where ω is the angular frequency, A is a constant, and the exponent s is a frequency-dependent parameter and has value less than unity. The ac conductivity was acquired by subtracting dc conductivity from the measured ac conductivity with an assumption that ac and dc conduction processes arise due to separate mechanism. The frequency exponent s was obtained from the straight-line fits by the least-square fitting procedure.

(ii) There is a gradual transition of the conductivity from frequency-dependent at power law regime to frequency-independent at dc conductivity dominant regime.

(iii) In addition, the conductivity is less temperature dependent at the power law regime compared to the dc conductivity regime.

The exponent s depends on ω and the dependency is particularly strong at high ω. The microscopic conduction obtained from the magnitude of s as a function of temperature is shown in Figure 7(b).

ZnO shows semiconducting behaviour due to the presence of Zn^{2+} ions and the O^{2-} vacancies and the dc electrical conduction occurs by the hopping of small polarons between these two valence states of ions. Various theories for the ac conduction of semiconductors have been proposed in the past. It is usually assumed the dielectric loss occurs because carrier motion is reflected to be localized within pair of sites.[24] In principle, two distinct processes have been proposed for the relaxation mechanism, namely quantum-mechanical tunneling (QMT) through the barrier and classical hopping over the barrier.[24,25]

The QMT theory predicts the following expression for the ac conductivity:

$$\sigma(\omega) = \frac{1}{3}\pi N^2(E_F)\alpha^{-5}e^2kT\omega\ln^4\left(\frac{1}{\omega\tau_0}\right), \quad (3)$$

where τ_o is a characteristic relaxation time, $N(E_F)$ is density of states at Fermi level, α^{-1} is the localization length. The frequency exponent s for QMT theory is given by $s = 1 - \frac{4}{\ln(\frac{1}{\omega\tau_o})}$. QMT model states that s of $\sigma(\omega)$ is temperature independent but frequency dependent. For example, s yields to 0.89 for $\omega = 10^4$ Hz and $\tau_0^{-1} = 10^{13}$ Hz which is independent of temperature. QMT theory is in disagreement with the temperature dependence of σ (ω). The experimental values of $\sigma(\omega)$ show stronger temperature dependence (as shown in Figure 7(a)) than predicted by QMT theory.

Alternatively, the experimental results of ZnO can be explained in terms of classical hopping theory. A classical model which assumes correlated barrier hopping (CBH) of electrons was developed by Elliot[25] and Pike.[26] The ac conductivity in CBH theory for single or bipolaron hopping is given by

$$\sigma_{ac}(\omega) = \frac{n\pi^3N^2\varepsilon\varepsilon_o\omega R_\omega^6}{24}, \quad (4)$$

where ε and ε_o are the dielectric constants of the materials and the free space, respectively. N is the concentration of pair sites, n is the number of electrons involved in the hopping process, $n = 1$ for single polaron hopping and $n = 2$ for bipolaron hopping, and R_ω is the hopping length which can be calculated from

$$R_\omega = \left(\frac{ne^2}{\pi\varepsilon\varepsilon_0}\right)\left(W_M + kT\ln\left(\frac{1}{\omega\tau_o}\right)\right), \quad (5)$$

where k is the Boltzmann constant and W_M is the maximum barrier height related to the relaxation variable W

$$W = W_M - \frac{e^2}{\pi\varepsilon\varepsilon_o R}, \quad (6)$$

where R is the intersite separation.

The temperature dependence of ac conductivity in ZnO-NPs at various frequencies is shown in Figure 8. It is observed that the conductivity increases with increasing temperature at all frequencies. The solid lines in the Figure 8 are the fitted parameter according to Eq. (4) with the value of $n = 2$. Thus, the CBH theory predicts quantitatively the temperature dependence of ac conductivity and its frequency exponent for the ZnO nanoparticles. Good agreement between the theoretical and experimental data confirmed that the ac conductivity in the ZnO-NPs is due to CBH bipolaron hopping.

TABLE III. Parameters obtained by fitting the experimental data to CBH theory for the ZnO-NPs.

W_M (eV)	τ_0 (s)	R_ω (Å)	N (cm^{-3})
0.91	7.51×10^{-11}	11.5	9.38×10^{25}

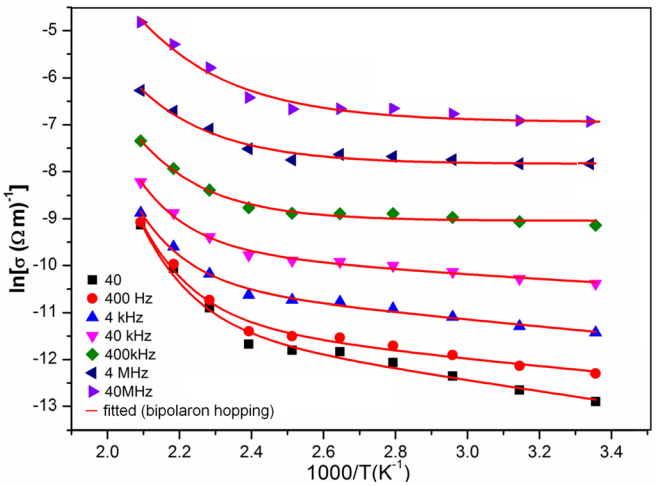

FIG. 8. Temperature dependence of ac conductivity of ZnO-NPs. The solid line represents fitted results of Eq. (3) with $n = 2$.

According to CBH model, the frequency exponent s is described as

$$s = 1 - \frac{6kT}{W_M - kT\ln\left(\frac{1}{\omega\tau_o}\right)}. \quad (7)$$

The solid line in the Figure 7(b) is the best fitted results according to Eq. (7). The fitting were performed using least square fitting technique (using ORIGIN PRO) with an assumption of fixed frequency ($\omega = 10^4$ s^{-1}) and the parameters, W_M and τ_0 obtained from the fitting are displayed in Table III. The maximum barrier height is calculated to be 0.91 eV and the hopping length of the polarons is ~11.5 Å. The ac conductivity data are fitted in Figure 8 by using the above obtained values of W_M and τ_0. It is noted that the fits appear to be reasonable over the entire temperature range measured. Moreover, the values of W_M, $\tau_{0,}$ and R_w obtained from the fitting are in marked agreement with the values published for ZnO nanorods[27] ($W_M = 0.92$ eV, $\tau_0 = 7.65 \times 10^{-10}$ s^{-1}, and $R_w \sim 12.7$ Å). Thus in the present investigation, the temperature dependence of ac conductivity and its frequency exponent for the ZnO nanoparticles is quite consistent with those predicted by CBH theory described above.

2. PU/ZnO nanocomposites

Figure 9 shows double logarithmic plots of real and imaginary components of complex permittivity ε^* against frequency f for PU/ZnO nanocomposites with ZnO-NPs of 0 to 15 vol. % at room temperature. As anticipated, the incorporation of ZnO-NPs into PU matrix modifies the dielectric spectra, where in all cases, the dielectric permittivity values obtained are higher than PU but lower than that of ZnO-NPs. The dielectric permittivity decreases as the frequency increases from 10 Hz to 10 kHz. The increase in the effective permittivity, ε_{eff} (the real permittivity of the composite), of the studied frequency region is attributed to the large permittivity of ZnO which enhanced the polarization from dipole-dipole interaction of closely packed nanoparticles.

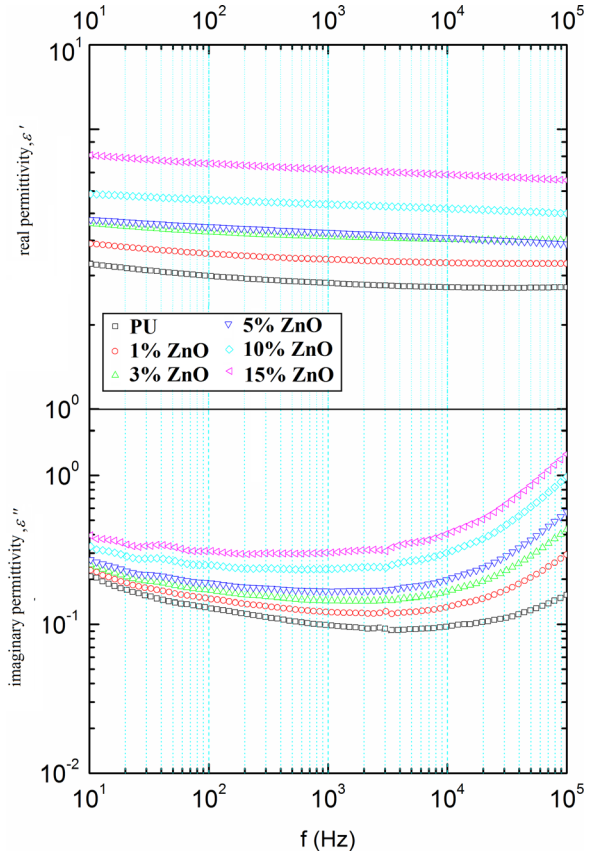

FIG. 9. Dielectric spectra of PU/ZnO nanocomposites with 0 to 15 vol. % of filler concentration at room temperature.

Predicting the ε_{eff} of PU/ZnO nanocomposites is very important for design of composite materials. In this case, the nanocomposites can be modeled by a two phase dispersion system consisting of continuous matrix (PU) and spherical inclusions (ZnO-NPs). ε_{eff} of such system can be predicted through a variety of theoretical models. These models are derived on the basis of various theoretical assumptions and experimental data. Figure 10 shows the room temperature dielectric constant of the nanocomposites at 100 Hz for different volume fractions of ZnO. The dielectric constants calculated based on the models discussed here is also included in the Figure 10 for comparison purposes. The fitting of the experimental results and theoretical model were accomplished using ORIGIN PRO 8.1. The Lichtenecker logarithmic law of mixing has been widely used for composite of two components

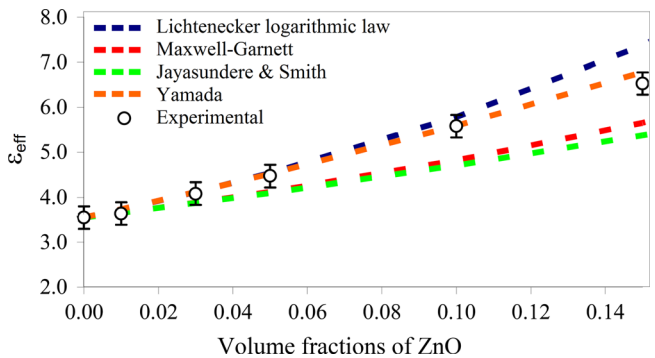

FIG. 10. Variation of effective dielectric constant (ε_{eff}) measured at room temperature and 100 Hz of PU/ZnO nanocomposites as a function of volume fraction of ZnO-NPs. The circles are experimental data and the solid lines are fit from various model.

$$\log \varepsilon_{eff} = (1-\phi)\log \varepsilon_1 + \phi \log \frac{\varepsilon_2}{\varepsilon_1}, \tag{8}$$

where ε_1 and ε_2 represent the dielectric permittivity of the polymer matrix (PU) and the ceramic inclusion (ZnO-NPs), respectively, and ϕ is the volume fraction of the inclusion. The mixing law is the intermediate form of series and parallel combination laws for dielectric mixture. This mixture law can be applied only if ε_1 differs slightly from ε_2.[28]

Another theoretical model which is widely used to predict dielectric constant between the permittivity of the various phases is Maxwell[29] model where the contrast between the permittivities of the phases is not very large. The effective dielectric constant based on Maxwell model is given as in Eq. (9).

$$\varepsilon_{eff} = \varepsilon_1 \left(\frac{2\varepsilon_1 + \varepsilon_2 + 2\phi(\varepsilon_2 - \varepsilon_1)}{2\varepsilon_1 + \varepsilon_2 - \phi(\varepsilon_2 - \varepsilon_1)} \right). \tag{9}$$

Effective permittivity may also be calculated from Jayasundere-Smith equation[30] (Eq. (10)), which was developed from Kerner's equation. Jayasundere and Smith applied a finite element model for two spheres having the same radius and this model is only valid when $\varepsilon_2 \gg \varepsilon_1$

$$\varepsilon_{eff} = \frac{(1-\phi)\varepsilon_1 + \phi\varepsilon_2 \left[\frac{3\varepsilon_1}{\varepsilon_2 + 2\varepsilon_1}\right]\left[1 + \frac{3\phi(\varepsilon_2 - \varepsilon_1)}{(\varepsilon_2 + 2\varepsilon_1)}\right]}{(1-\phi) + \phi\left[\frac{3\varepsilon_1}{\varepsilon_2 + 2\varepsilon_1}\right]\left[1 + \frac{3\phi(\varepsilon_2 - \varepsilon_1)}{(\varepsilon_2 + 2\varepsilon_1)}\right]}. \tag{10}$$

In addition to mixing rules suggested above, there are also mixing formulae which contain adjustable parameters which takes into consideration the morphology of the particles. Yamada and his coworkers have proposed a model for binary system consist of lead zirconate titanate, PZT powder embedded in a polymer matrix of polyvinylidene fluoride, PVDF.[31] Dielectric constant of the composites based on Yamada equation is given by

$$\varepsilon_{eff} = \varepsilon_1 \left[1 + \frac{\phi(\varepsilon_2 - \varepsilon_1)}{\varepsilon_1 + n(\varepsilon_2 - \varepsilon_1)(1-\phi)} \right], \tag{11}$$

where $n(=1/\eta)$ is the morphology fitting constant, corresponds to the shape of ellipsoidal particle and their orientation in relation to composite film surface material. The value of n is greatly affected by the change in the morphology factor.

Comparison between the experimental value and the theoretical models show that all the models mentioned above are in good agreement with the experimental data only up to $\phi = 0.03$ of ZnO-NPs. Above $\phi = 0.03$, the Jayasundere-Smith and Maxwell are not suitable to predict ε_{eff} because the theoretical data deviate ($\sim$>8% deviations) from the experimental value.

As for Lichtenecker equation, ε_{eff} of PU/ZnO nanocomposite is linearly proportional to ϕ up to 0.10 but there is a deviation of $\sim$13% for $\phi = 0.15$. Lichtenecker equation

appears to be useful for predictions of ε_{eff} for PU/ZnO nanocomposites with the limitation up to $\phi = 0.10$.

As for Yamada model, the experimental values fit well with the shape parameter of $n = 0.19$ for the entire volume fraction of ZnO studied in the present study. For instance, the value of ε_{eff} (6.78) for $\text{ø} = 0.15$ is comparable to the experimental ε_{eff} (6.53).

The goal of this investigation was to devise a model that can accurately account for the dielectric properties of the PU/ZnO thins films particularly at definite volume fraction with parameters of clear physical meaning. The observations clearly demonstrate the effective applicability of Yamada model to rationalize the dielectric characteristics of the present composite up to 0.15 filler content.

IV. CONCLUSIONS

ZnO-NPs and the nanocomposite thin films of PU/ZnO with ZnO-NP content of 0%–15% were characterized. Morphology and structures of the prepared samples were analyzed through TEM, SEM, and FTIR. The FTIR results indicated that hydroxyl groups on ZnO-NPs reacted with isocyanates groups, thus improve the compatibility between ZnO and the polyurethane matrix. The dielectric relaxation mechanism of ZnO was due to interfacial polarization at lower frequencies and orientational polarization at higher frequencies. The dielectric constant of ZnO-NPs increased with increasing temperature. The ac conductivities were analyzed through power law relation. The transport behaviour of the ZnO-NPs have been investigated and compared with theoretical models. Bipolaron hopping CBH model is an appropriate mechanism for the AC conductivity in the temperature range inspected. As for the PU/ZnO nanocomposites, the inclusion of ZnO-NPs on the PU matrix significantly increases the effective dielectric permittivity of the nanocomposites. Various models are used for rationalizing the dielectric behaviour of the nanocomposites. Among them, the Yamada equation gives a satisfactory prediction for the effective permittivity of these nanocomposites over the frequency range up to 15 vol. % of inclusion.

ACKNOWLEDGMENTS

Grants from UM.C/625/1/HIR/041, Vot. F F016/2004, and UM.C/HIR/MOHE/SC/06 are acknowledged for supporting this work. The authors wish to thank Professor Takeo Furukawa for his valuable discussion.

[1]M. S. Samuel *et al*., Curr. Appl. Phys. **11**, 1094 (2011).
[2]Y. Zong, Y. Cao, D. Jia, S. Bao, and Y. Lu, Mater. Lett. **64**, 243 (2010).
[3]M. S. Samuel *et al*., Physica B **406**, 3023 (2011).
[4]C. K. N. Peh *et al*., Mater. Lett. **64**, 1372 (2010).
[5]T. Minami, J. Vac. Sci. Technol. A **17**, 1765 (1999).
[6]D. Kanda *et al*., J. Mater. Sci. **43**, 5436 (2008).
[7]J. Zheng *et al*., Polymer **47**, 7786 (2006).
[8]G. Georgoussis *et al*., Eur. Polym. J. **35**, 2007 (1999).
[9]J. Zheng *et al*., Polymer **46**, 10873 (2005).
[10]R. S. Mishra *et al*., Eur. Polym. J. **45**, 960 (2009).
[11]A. K. Mishra *et al*., Prog. Org. Coat. **67**, 405 (2010).
[12]L. H. Yang *et al*., Prog. Org. Coat. **53**, 91 (2005).
[13]S. K. Bhattacharya and R. R. Tummala, J. Mater. Sci.: Mater. Electron. **11**, 253 (2000).
[14]S. K. Bhattacharya and R. R. Tummala, Microelectron. J. **32**, 11 (2001).
[15]Y. Rao *et al*., J. Appl. Polym. Sci. **83**, 1084 (2002).
[16]S. K. Bhattacharya, Mater. Sci. Eng., B **110**, 233 (2004).
[17]A. K. Zak *et al*., Mater. Lett. **65**, 70 (2011).
[18]T. S. Velayutham *et al*., J. Appl. Polym. Sci. **112**, 3554 (2009).
[19]T. S. Velayutham *et al*., Prog. Org. Coat. **66**, 367 (2009).
[20]I. Yilgor *et al*., Polymer **47**, 4105 (2006).
[21]K. K. Jena *et al*., Eur. Polym. J. **43**, 1825 (2007).
[22]M. K. Gupta *et al*., Mater. Lett. **63**, 1910 (2009).
[23]A. K. Jonscher, *Dielectric Relaxation in Solids* (Chelsea Dielectrics, London, 1983).
[24]P. Extance *et al*., Phys. Rev. B **32**, 8148 (1985).
[25]S. R. Elliot, Adv. Phys. **36**, 135 (1987).
[26]G. E. Pike, Phys. Rev. B. **6**, 1572 (1972).
[27]M. S. Samuel *et al*., J. Appl. Phys. **109**, 113702 (2011).
[28]K. Mazur, Plast. Eng. **28**, 539 (1995).
[29]J. C. Maxwell, *A Treatise on Electricity and Magnetism* (Dovel, New York, 1954).
[30]N. Jayasundere and B. V. Smith, J. Appl. Phys. **73**, 2462 (1993).
[31]T. Yamada *et al*., J. Appl. Phys. **53**, 4328 (1982).